Vol. 522: 15–32, 2015
doi: 10.3354/meps11156

MARINE ECOLOGY PROGRESS SERIES
Mar Ecol Prog Ser

Published March 2

Community structure of under-ice fauna in the Eurasian central Arctic Ocean in relation to environmental properties of sea-ice habitats

Carmen David[1,2,*], Benjamin Lange[1,2], Benjamin Rabe[1], Hauke Flores[1,2]

[1]Alfred Wegener Institut Helmholtz-Zentrum für Polar- und Meeresforschung, Am Handelshafen 12, 27570 Bremerhaven, Germany

[2]University Hamburg, Centre for Natural History (CeNak), Zoological Museum, Biocenter Grindel, Martin-Luther-King Platz 3, 20146 Hamburg, Germany

ABSTRACT: Arctic sea-ice decline is expected to have a significant impact on Arctic marine ecosystems. Ice-associated fauna play a key role in this context because they constitute a unique part of Arctic biodiversity and transmit carbon from sea-ice algae into pelagic and benthic food webs. Our study presents the first regional-scale record of under-ice faunal distribution and the environmental characteristics of under-ice habitats throughout the Eurasian Basin. Sampling was conducted with a Surface and Under-Ice Trawl, equipped with a sensor array recording ice thickness and other physical parameters during trawling. We identified 2 environmental regimes, broadly coherent with the Nansen and Amundsen Basins. The Nansen Basin regime was distinguished from the Amundsen Basin regime by heavier sea-ice conditions, higher surface salinities and higher nitrate + nitrite concentrations. We found a diverse (28 species) under-ice community throughout the Eurasian Basin. Change in community structure reflected differences in the relative contribution of abundant species. Copepods (*Calanus hyperboreus* and *C. glacialis*) dominated in the Nansen Basin regime. In the Amundsen Basin regime, amphipods (*Apherusa glacialis*, *Themisto libellula*) dominated. Polar cod *Boreogadus saida* was present throughout the sampling area. Abrupt changes from a dominance of ice-associated amphipods at ice-covered stations to a dominance of pelagic amphipods (*T. libellula*) at nearby ice-free stations emphasised the decisive influence of sea ice on small-scale patterns in the surface-layer community. The observed response in community composition to different environmental regimes indicates potential long-term alterations in Arctic marine ecosystems as the Arctic Ocean continues to change.

KEY WORDS: Arctic · Under-ice habitats · *Calanus* · Ice-associated amphipods · Polar cod · *Boreogadus saida* · *Apherusa glacialis*

INTRODUCTION

The Arctic Ocean is experiencing some of the most pronounced effects of global climate change (Arctic Climate Impact Assessment 2004). During the past 4 decades, reductions in sea-ice concentration and thickness and in the duration of the melting season have been recorded in the Arctic Ocean (Rigor & Wallace 2004, Shimada et al. 2006, Kwok & Rothrock 2009, Markus et al. 2009, Stroeve et al. 2012, Overland & Wang 2013) and are predicted to continue in the future (Johannessen et al. 2004, Polyakov et al. 2005, Stroeve et al. 2007). The Arctic Ocean is changing from a perennial multi-year ice (MYI)-dominated system to a seasonal first-year ice (FYI) system (Maslanik et al. 2011). In 2012, the sea-ice extent was

*Corresponding author: carmen.david@awi.de

reduced to approximately half of the mean for the past 4 decades, resulting in large open-water areas (Parkinson & Comiso 2013).

These changes are expected to result in modifications of the biological systems in the Arctic Ocean. Reduction in the extent and thickness of sea ice leads to more light availability in the water column, which has been hypothesised to induce a net increase in primary production (Arrigo et al. 2008, Arrigo & van Dijken 2011). This may be true on the shelves where nutrient supply by advection or vertical mixing can be extensive. Over the basins, however, primary production can be nutrient-limited due to strengthened stratification by ice melt (Tremblay & Gagnon 2009). Sea-ice loss will lead to a decrease in ice algal production, which can account for up to 50% of the primary production in the central Arctic Ocean (Gosselin et al. 1997). Ice algae are considered a high-quality food source for Arctic marine food webs (Søreide et al. 2006, 2013). How these changes in primary production will impact marine fauna is an open question. The number of documented changes in Arctic planktonic systems is low, and the number reported from the central Arctic Ocean is even lower (Wassmann et al. 2011). Lack of biological baseline data makes it impossible to estimate the effect of recent environmental changes on the biological system (Kosobokova & Hirche 2000). Increasing efforts have been made in recent years to investigate zooplankton distribution at different scales (Hopcroft et al. 2005, Matsuno et al. 2012, Hunt et al. 2014, Pomerleau et al. 2014). Only recently have zooplankton data from different Arctic cruises been compiled into a large-scale analysis, providing a first baseline to monitor the influence of environmental change on the Arctic pelagic system (Kosobokova & Hirche 2009). It should be borne in mind, however, that this dataset dates from the 1990s, a period when environmental change in the Arctic Ocean was already ongoing.

Most affected by environmental changes are the organisms living in association with sea ice. Ice-associated fauna have been described as those species that complete their entire life cycle within the sea ice or spend only part of their life cycle associated with sea ice (Melnikov & Kulikov 1980). Many uncertainties still remain in understanding the association of these organisms with sea-ice habitats. Community structure of ice-associated fauna is assumed to be related to ice age, density and under-ice topography (Hop et al. 2000a, Hop & Pavlova 2008). Ice-associated species may prefer a certain type of ice, e.g. MYI or FYI (Hop et al. 2000a). Some, such as the large amphipod *Gammarus wilkitzkii*, are found associated with ridges, which provide shelter during the melting season (Hop & Pavlova 2008, Gradinger et al. 2010). The widely distributed amphipod *Apherusa glacialis* prefers flat ice floes (Hop & Pavlova 2008), or ice edges (Hop et al. 2000b, Beuchel & Lønne 2002).

Crucial for the functioning of the Arctic ecosystem is the role of ice-associated fauna in the energy transfer to higher trophic levels (Budge et al. 2008). The dominance of diatom fatty acid trophic markers in the lipids of calanoid copepods and ice-associated amphipods underpins the importance of sea-ice algae as a critical carbon source in Arctic food webs (Budge et al. 2008, Falk-Petersen et al. 2009). Feeding extensively on calanoid copepods (Scott et al. 1999, Benoit et al. 2010) and amphipods (Matley et al. 2013), polar cod *Boreogadus saida* in turn represents a preferential prey for seabirds and marine mammals (Bradstreet & Cross 1982, Finley & Gibb 1982, Welch et al. 1992). As a key species of the Arctic system, the polar cod is believed to account for up to 75% of the energy transfer between zooplankton and vertebrate predators (Welch et al. 1992). Ice algae–copepods/amphipods–polar cod–top predators represents probably one of the most efficient pathways in energy flux through the Arctic food web, yet all its components are closely related with sea ice (Scott et al. 1999, Harter et al. 2013, Hop & Gjøsæter 2013). Changes in composition, abundance, size and energy content of ice-associated communities will influence the energy flux through the Arctic marine ecosystem and, hence, the growth and survival of top predators (Mehlum & Gabrielsen 1993, Laidre & Heide-Jørgensen 2005). Therefore, an accurate quantification of ice-associated fauna on large spatial scales is crucial to understand the functioning of Arctic sea-ice-dependent ecosystems and their future fate. The sea-ice-covered Arctic Ocean, however, is difficult to access. In particular, sampling under the sea ice is challenging. Most commonly, ice-associated macrofauna have been sampled by divers (Arndt & Pavlova 2005, Hop et al. 2011). This method is excellent in describing the small-scale structure of ice habitats during sampling, yet the spatial variability of the organism distributions may not be covered representatively. Ice floes which appear biologically poor are not sampled due to limited time at ice stations, while it is impossible to obtain all organisms from ice floes with rich fauna (Hop & Pavlova 2008). A new sampling gear used in the Southern Ocean for the first time, the Surface and Under-Ice Trawl (SUIT) (van Franeker et al. 2009), overcomes the spatial limita-

tion of observations by divers (Flores et al. 2012). SUIT enables large-scale horizontal sampling of the 0–2 m surface layer both under sea ice and in open water.

The aim of the present study is to describe the association of macrofaunal communities in the surface layer (0–2 m) under ice and in open water, with habitat properties of the sea ice and the underlying water column. In particular we address the following objectives:

(1) We identify key environmental variables of the sea ice and water column that structure under-ice habitats.

(2) We provide a basin-wide inventory of under-ice fauna in the Eurasian central Arctic Ocean and highlight key species defining the under-ice communities.

(3) We investigate the role of under-ice habitat properties in structuring the under-ice community.

MATERIALS AND METHODS

Study area and sampling technique

Sampling was performed during RV 'Polarstern' expedition ARK XXVII/3 (2 August–29 September 2012) across the ice-covered Eurasian part of the Arctic Ocean deep-sea basin, from 82 to 89° N and 30 to 130° E (Fig. 1). Thirteen horizontal hauls were performed under different ice types (MYI, FYI) and in open water. Sampling was performed with an improved version of SUIT (van Franeker et al. 2009). The improved SUIT consisted of a steel frame with a 2 × 2 m opening and 2 parallel 15 m long nets attached: (1) a 7 mm half-mesh commercial shrimp net, lined with 0.3 mm mesh in the rear 3 m of the net, covered 1.5 m of the opening width and (2) a 0.3 mm mesh zooplankton net, covered 0.5 m of the opening width. Floats attached to the top of the frame kept the net at the surface or the sea-ice underside. To enable sampling under undisturbed ice, an asymmetric bridle forces the net to tow off at an angle of approximately 60° to starboard of the ship's track, at a cable length of 150 m. A detailed description of SUIT sampling performance is provided as supplementary material by Flores et al. (2012). Depending on the ice conditions, SUIT haul durations varied between 3 and 38 min, with a mean of 24 min.

Environmental data

A sensor array was mounted in the SUIT frame, consisting of an acoustic Doppler current profiler (ADCP), a conductivity-temperature-depth probe (CTD) with built-in fluorometer, an altimeter, 2 spectral radiometers and a video camera. Water inflow speed was estimated using a Nortek Aquadopp® ADCP. Three acoustic beams operating at a frequency of 2 MHz allowed construction of 3-dimensional profiles of the currents in the net opening. The ADCP measured the current velocity at 3 locations across the SUIT opening. The ADCP was also equipped with sensors for pressure, pitch, role and heading. These data were used to reconstruct the position of the SUIT in the water during each haul as an indicator of the catch performance. Temperature and salinity profiles were obtained with a Sea and Sun CTD75M probe. The practical salinity scale (PSS-78) was used for salinity values (Fofonoff 1985). A built-in Turner cyclops fluorometer was used to estimate the under-ice chlorophyll concentration. Calibration of fluorometric chlorophyll *a* concentrations was

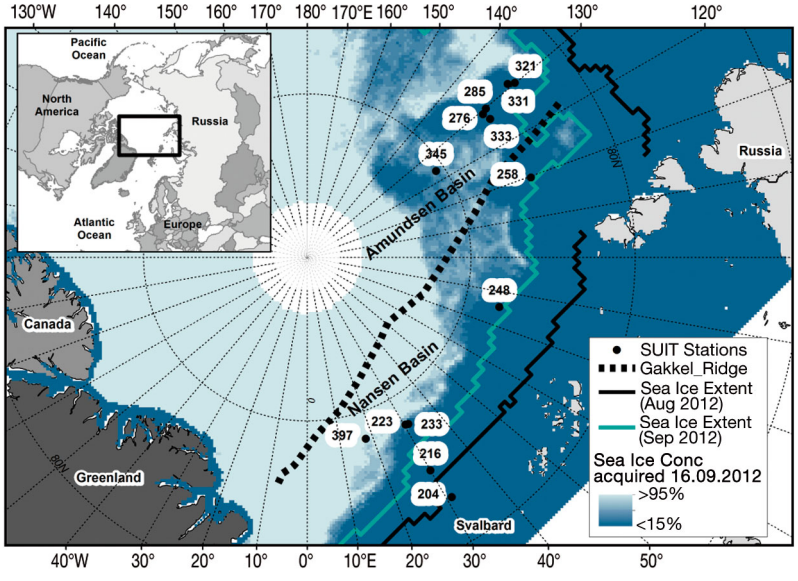

Fig. 1. SUIT (Surface and Under-Ice Trawl) station map during RV 'Polarstern' expedition IceARC (ARK XXVII/3). Sea-ice concentration on 16 Sept 2012 (data acquired from Bremen University; www.iup.uni-bremen.de:8084/amsr/) and mean sea-ice extent for August and September 2012 are represented on the map (data acquired from NSIDC; Fetterer et al. 2002). Number codes next to sampling locations indicate station numbers

done from water samples obtained during stationary sea-ice work. The calibration coefficients were derived from the linear relationship between chlorophyll *a* concentrations of water samples (measured with high-pressure liquid chromatography), with fluorometric chlorophyll *a* concentrations of the corresponding 1 m depth range (n = 2484; adj. $r^2 = 0.63$; $p < 0.001$). Data gaps in the CTD measurements caused by low battery voltage were filled using complementary datasets from the ADCP data (pressure) and the shipboard sensors (temperature and salinity), using correction factors determined by linear regression. An altimeter Tritech PA500/6-E connected to the CTD probe measured the distance between the net and the sea-ice underside. Sea-ice draft was calculated as the difference between the depth of the net relative to the water level, measured by the CTD pressure sensor, and the distance to the sea-ice underside, measured by the altimeter, and corrected for pitch and roll angles. Draft was then converted into ice thickness by using a sea-ice density value of 834 kg m^{-3}, determined from sea-ice core samples.

During each haul, changes in ship speed, ice concentration (%) and irregularities were estimated visually by an observer on deck. GPS waypoints were recorded by the observer when the SUIT was deployed and hauled in, when it behaved abnormally, or when the environment changed, e.g. when the SUIT entered or exited the sea ice. The distance sampled over ground was estimated by multiplying the amount of time the SUIT was in the water (s) with the average speed in water (m s^{-1}). The distance sampled under ice was estimated in an analogue way for the period during which the SUIT was under ice. The sampled ice coverage was then expressed as percentage distance sampled under ice of the total distance sampled over ground.

Gridded daily sea-ice concentrations for the Arctic Ocean derived from SSMIS satellite data using the algorithm specified by Spreen et al. (2008) were downloaded from the sea-ice portal of the University of Bremen (www.meereisportal.de).

A CTD probe with a carousel water sampler was used to collect environmental parameters from the water column near SUIT stations. The CTD (Seabird SBE9+) was equipped with a seafloor altimeter (Benthos), a fluorometer (Wetlabs FLRTD), a dissolved oxygen sensor (SBE 43) and a transmissiometer (Wetlabs C-Star). Details of the CTD sampling procedure were provided in Boetius et al. (2013). Data are available online in the PANGEA database (Rabe et al. 2012). Among all CTD stations, the closest in time and space to the SUIT stations were chosen (Table 1). Nutrients were analysed in an air-conditioned laboratory container with a continuous flow auto-analyser (Technicon TRAACS 800) following the procedure described in Boetius et al. (2013). Measurements were made simultaneously on 4 channels: PO_4, Si, NO_2 + NO_3 together and NO_2 separately.

The depth of the upper mixed layer was calculated from the ship CTD profiles after Shaw et al. (2009), who define the depth of the mixed layer as the depth of the profile where the density difference to the surface exceeds 20% of the density difference between 100 m and the surface.

Table 1. Station table of Surface and Under-Ice Trawls (SUITs) and the corresponding conductivity-temperature-depth (CTD) stations. Station date given as mo/d/yr

Haul	Basin	SUIT					CTD			
		Station code	Station date	Latitude (°N)	Longitude (°E)	Bottom depth (m)	Station code	Station date	Latitude (°N)	Longitude (°E)
1	Nansen	204	8/5/2012	81.450	31.098	423	208	8/6/2012	81.462	31.038
2	Nansen	216	8/7/2012	82.483	30.027	3610	215	8/7/2012	82.488	30.001
3	Nansen	223	8/9/2012	84.070	30.434	4016	227	8/9/2012	84.026	31.225
4	Nansen	233	8/11/2012	84.045	31.298	4011	227	8/9/2012	84.026	31.225
5	Nansen	248	8/16/2012	83.934	75.500	3424	242	8/16/2012	83.902	76.067
6	Nansen	258	8/20/2012	82.743	109.627	3575	254	8/20/2012	82.696	109.119
7	Amundsen	276	8/25/2012	83.076	129.125	4188	281	8/26/2012	82.893	129.826
8	Amundsen	285	8/26/2012	82.896	129.782	4174	281	8/26/2012	82.893	129.826
9	Amundsen	321	9/4/2012	81.717	130.033	4011	324	9/4/2012	81.925	131.120
10	Amundsen	331	9/5/2012	81.905	130.863	4036	324	9/4/2012	81.925	131.120
11	Amundsen	333	9/6/2012	82.989	127.103	4187	333	9/6/2012	83.003	127.177
12	Amundsen	345	9/9/2012	85.254	123.842	4354	342	9/9/2012	85.158	123.349
13	Nansen	397	9/29/2012	84.172	17.922	4028	387	9/28/2012	84.368	17.525

The relative light intensity was calculated by dividing the solar elevation angle during the SUIT haul by the solar elevation angle at solar maximum for the corresponding location. Solar elevation angles were calculated using the National Oceanic and Atmospheric Administration's (NOAA) online solar calculator with latitude, longitude, date and time as inputs (www.esrl.noaa.gov/gmd/grad/solcalc/).

Biological data

The catch was partially sorted on board. Polar cod and ctenophores were immediately extracted from samples. The remaining samples from the shrimp and zooplankton nets were then each equally divided into 2 parts with a plankton splitter (Motoda 1959). From each sample, part of the material was immediately preserved in 4% formaldehyde/seawater solution for quantitative analysis. After the cruise, the quantitative samples were analysed for species composition and density at the Alfred Wegener Institute in Bremerhaven, Germany. Macrofauna (>0.5 cm) densities were derived from the analysis of the shrimp net samples. Copepod densities were derived from analysis of the zooplankton net samples. With few exceptions, all animals were identified to the species level and, in copepod species, to developmental stage and sex. The adult copepods and their larger juvenile stages (the copepodite CV and CIV) were both considered in density calculations. Densities were calculated dividing the total number of animals per haul by the trawled area. The trawled area was calculated by multiplying the distance sampled in water, estimated from ADCP data (Flores et al. 2011), with the net width (0.5 m for the zooplankton net and 1.5 m for the shrimp net).

Data analysis

Scatterplots between each possible combination of 2 environmental variables were used to identify pairs of datasets with high colinearity (Zuur et al. 2007). In pairs with Spearman's rank correlation coefficients >0.7, only 1 variable was chosen for subsequent analysis based on the ecological relevance to the scientific objectives of this study and the comparability with other studies. From a total of 30 variables analysed, 12 were retained for further statistical analysis (Table 2). A principal component analysis (PCA) (Mardia et al. 1979) was applied on the environmental dataset to reveal patterns in habitat typologies according to properties of the sea ice and the underlying water column.

In order to investigate patterns of diversity over the sampling area, 3 diversity indices were calculated for the whole biological dataset, as well as for sub-groupings derived from environmental data analysis: (1) species richness (the number of species observed at each station) (S), (2) the Shannon index (H) (Shannon 1948) and (3) Pielou's evenness index (J). Species accumulation curves were plotted to assess the impact of sampling effort on species diversity. To assess the statistical difference between sub-groupings, the Mann-Whitney test was performed on diversity indices and on cumulated species densities at stations (Mann & Whitney 1947).

Species density data were analysed using non-metric multidimensional scaling (NMDS) (Kruskal 1964) based on a Bray-Curtis similarity matrix (Bray & Curtis 1957). NMDS is commonly regarded as the most robust unconstrained ordination method in community ecology (Minchin 1987). Square-root transformations and Wisconsin double standardization were applied to the data to gradually down-

Table 2. Environmental variables characterising sea-ice habitats. SUIT: Surface and Under-Ice Trawls

Variable (abbreviation)	Unit	Value range
Sampled ice coverage during SUIT hauls (Coverage)	%	0 to 100
Modal ice thickness (Thickness)	m	0 to 1.25
Standard deviation of ice thickness (SD)	m	0 to 0.88
Surface-water temperature (Temperature)	°C	−1.76 to −1.06
Surface salinity (Salinity)		29.38 to 32.87
Chlorophyll *a* concentration at the surface (Chl*a*-surface)	mg m^{-3}	0.06 to 0.24
Chlorophyll *a* concentration at the depth of the chlorophyll *a* maximum (Chl*a*)	mg m^{-3}	0.15 to 0.63
Silicate concentration at the depth of the chlorophyll *a* maximum (Si)	µmol l^{-1}	1.17 to 4.80
Combined nitrate + nitrite concentration at the depth of the chlorophyll *a* maximum (NO_x)	µmol l^{-1}	0.12 to 6.84
Phosphate concentration at the depth of the chlorophyll *a* maximum (PO_4)	µmol l^{-1}	0.20 to 0.55
Relative daylight intensity (Relative light)	–	0 to 0.91
Mixed-layer depth (MLD)	m	9 to 25

weight the dominant taxa. The performance of the NMDS was assessed with Shepard plots and stress values (Clarke 1993, Legendre & Legendre 2012). ANOSIM (Clarke & Ainsworth 1993) was used to test for significant differences in the community structure between *a priori* defined groupings, e.g. ocean basins and ice regimes.

The association of the community structure with the physical environment was evaluated with a Mantel test (Mantel 1967). The Mantel test relates 2 distance matrices, one from the biological and one from the environmental dataset, using Pearson correlation (Smouse et al. 1986). The bootstrapping procedure was applied with 999 iterations. Afterwards, the association of the community structure with all possible combinations of environmental variables was evaluated with the BioEnv analysis (Clarke & Ainsworth 1993). The BioEnv analysis estimates the subset of environmental variables that has the highest correlation with the biological data. The best subset was found using the Spearman's rank correlation coefficient between a Bray-Curtis similarity matrix of the species density data and a Euclidean dissimilarity matrix of the environmental variables.

For all analyses, R software Version 3.1.2 was used with the libraries vegan, FactoMineR, plyr and MASS (R Core Team 2014).

RESULTS

Environmental conditions

Across the Eurasian Basin 13 stations were sampled. Seven stations were located in the Nansen Basin, and 6 stations in the Amundsen Basin. Six of the Nansen Basin stations were sampled during the first half of August, and the Amundsen Basin stations during late August to mid-September. The last station was sampled in the Nansen Basin on 29 September 2012 at the onset of winter (Table 1). All stations had water depths >3400 m, except Stn 204 in the Nansen Basin, which was located in open waters over the continental slope at a depth of 423 m. Because oceanographic conditions at the slope station differed markedly from those in the rest of the sampling area, it was not included in the multivariate analysis, but is discussed separately. Besides Stn 204 in the Nansen Basin, 2 of the Amundsen Basin stations were nearly ice-free. At all other stations sea ice was present, ice coverage ranging from 56 to 100% (Fig. 2A). Modal ice thickness ranged from 0.45 to 1.25 m. Within the deep-sea basins, surface temperatures ranged between −1.8 and −1°C. The surface temperature at the slope station (Stn 204) was 0.8°C (Fig. 2A).

In the PCA of physical variables, 63.6% of the variance in the dataset was explained on the first 2 axes (Fig. 3). The first axis explained 36.6% of the variance and was mainly driven by gradients of nutrients, salinity and sea-ice properties. Along this axis a clear distinction was evident between 2 environmental clusters that corresponded to the stations situated in the Nansen Basin and the Amundsen Basin, respectively. Because the environmental gradients in our dataset represent not only spatial patterns, but also an often inseparable temporal signal over the 2 mo sampling period, the clusters are referred to as spatio-temporal 'regimes', roughly corresponding to the 2 ocean basins. Sea-ice coverage and thickness gradients increased towards the Nansen Basin regime. The 2 open-water stations in the Amundsen Basin were clearly distinguished from all other stations, and were associated with the lowest sea-ice coverage and thickness values. Furthermore, the Nansen Basin regime was associated with high values of salinity and nitrate + nitrite, and low values of silicate and chlorophyll *a* concentrations in the 0–2 m surface layer. Conversely, the Amundsen Basin regime was associated with high chlorophyll *a* concentrations, high silicate concentrations, and low values of salinity and nitrate + nitrite. The second axis explained 26.94% of the variance and was mainly associated with gradients of temperature, chlorophyll *a* concentration at the chlorophyll maximum depth and relative light intensity. Along this axis, 2 stations were distinguished from the Nansen Basin regime cluster. Stn 216 had 100% ice coverage, high surface-water temperatures and high chlorophyll *a* concentrations at the chlorophyll maximum depth (Fig. 2). Stn 397 had the lowest surface-water temperatures and lowest relative light intensity. The open-water station (Stn 333) was distinguished along the second axis from the cluster of the Amundsen Basin regime by high surface-water temperatures and high chlorophyll *a* concentrations at the chlorophyll maximum depth.

When single environmental parameters were compared between the 2 regimes, surface salinity was significantly higher in the Nansen Basin regime (30–33) than in the Amundsen Basin regime (29–31) ($W = 0$, p-value < 0.01) (Fig. 2B). The mixed-layer depth (MLD) was shallowest at the first ice station (Stn 216; 9 m), which was situated at the ice edge. At the beginning of the cruise in the Nansen Basin regime, the MLD was around 15 m deep and in-

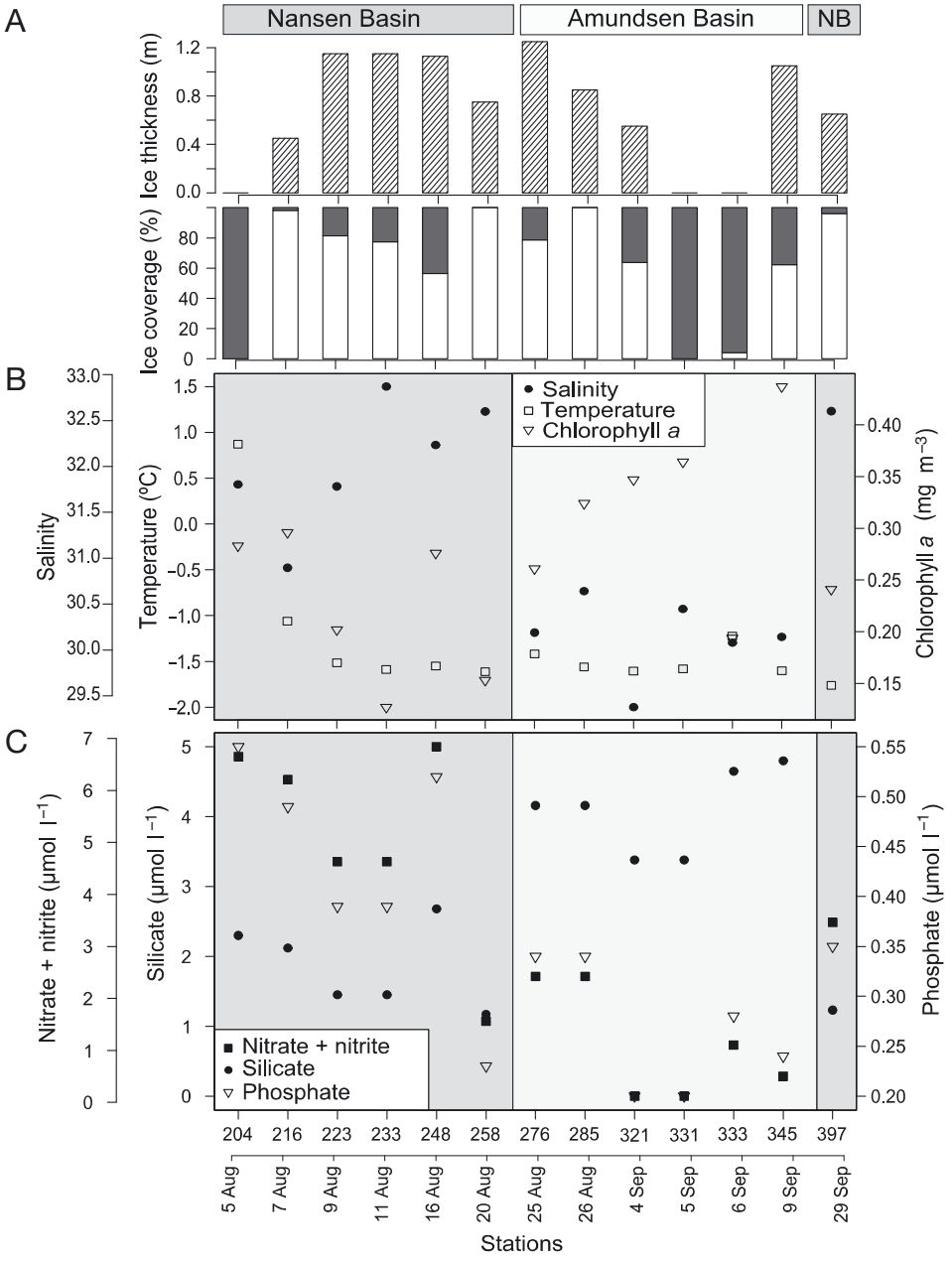

Fig. 2. Environmental variables recorded at sampling stations. (A) Ice thickness (upper panel) and ice coverage (lower panel). White portion of bars: percentage of sea-ice coverage at each station; grey portion of bars: remaining percentage of open water at each station. (B) Temperature, salinity and chlorophyll *a* concentration in the 0–2 m surface layer. (C) Nutrient concentrations at the depth of the chlorophyll *a* maximum. Nansen Basin stations are shown on dark grey background, and Amundsen Basin stations on light grey background

creased with time, reaching up to 30 m in the Amundsen Basin regime. At the last station sampled in the Nansen Basin regime (Stn 397), the MLD was again shallower. High average values of nitrate + nitrite (4.8 µmol l^{-1}) and phosphate (0.4 µmol l^{-1}) and low values of silicate (1.7 µmol l^{-1}) characterised surface waters of the Nansen Basin regime (Fig. 2C). The opposite conditions were encountered in the Amundsen Basin regime, with low values of nitrate + nitrite (1.4 µmol l^{-1}) and phosphate (0.2 µmol l^{-1}) and high values of silicate (3.5 µmol l^{-1}). The differences between the 2 regimes in nutrient concentration were statistically significant (NO_x: $W = 2$, p-value < 0.01; PO_4: $W = 4$, p-value < 0.05; Si: $W = 36$, p-value < 0.01).

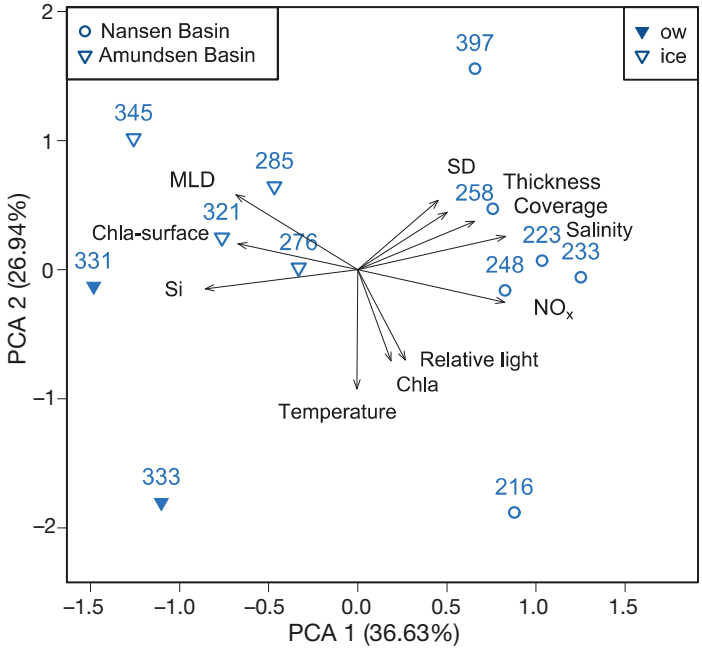

Fig. 3. Principal component analysis of environmental variables at the sampling stations. Variable labels as defined in Table 2. Nansen Basin stations are represented by circles; Amundsen Basin stations are represented by triangles—ice: under-ice stations; ow: open-water stations. Percentage values on the axes represent the explained variance on the first (PCA 1) and second (PCA 2) dimensions. Other abbreviations as in Table 2

At the station positioned over the Gakkel Ridge (Stn 258), all nutrients had very low concentrations. At the 2 open-water stations in the Amundsen Basin regime (Stns 331 and 333), nitrate + nitrite and phosphate were depleted in the surface waters. The averaged surface chlorophyll *a* concentration over the entire sampling area was 0.27 mg m^{-3}, ranging between 0.12 and 0.43 mg m^{-3}. The surface chlorophyll *a* concentrations were slightly higher in the Amundsen Basin regime than in the Nansen Basin regime (W = 30, p-value < 0.1). The highest value was found at Stn 345 in the Amundsen Basin regime (Fig. 2B).

Taxonomic composition

In total, 28 species belonging to 10 phyla were identified in our samples (Table 3). Copepods had the highest densities, accounting for 69% of the mean relative density over all stations, followed by amphipods with 28% (Fig. 4). The balance between copepods and amphipods, however, was markedly different between the 2 environmental regimes: in the Nansen Basin regime, copepods accounted for >82% of the mean density, whereas, in the Amundsen Basin regime, copepods contributed only 53%. Here the amphipods co-dominated the species composition, accounting for 43% of the mean density (Fig. 4). Appendicularians contributed 1.3% to the overall density, but this value was driven by extremely high densities at only 2 stations. Ctenophores had a high frequency of occurrence over the entire sampling area, but with highly variable densities. At 2 stations ctenophores heavily dominated the biomass of the samples. The other taxonomic groups accounted for <1% of the density.

Variability in species diversity, density and distribution

The highest number of species (20) was encountered at Stn 285 in the Amundsen Basin regime. Three other stations, 2 situated in the Nansen Basin regime and 1 in the Amundsen Basin regime, had 19 species each. The lowest species richness (S), Shannon diversity (H) and evenness (J) were encountered at the slope station (Stn 204), where only 8 species were found (Table 4). The highest Shannon and evenness indices were encountered at an open-water station (Stn 331) in the Amundsen Basin regime. Species richness and Shannon diversity showed no significant difference between the 2 environmental regimes (S: W = 29, p-value > 0.1; H: W = 32, p-value < 0.1), while species evenness (J) was significantly higher in the Amundsen Basin than in the Nansen Basin (W = 34, p-value < 0.05).

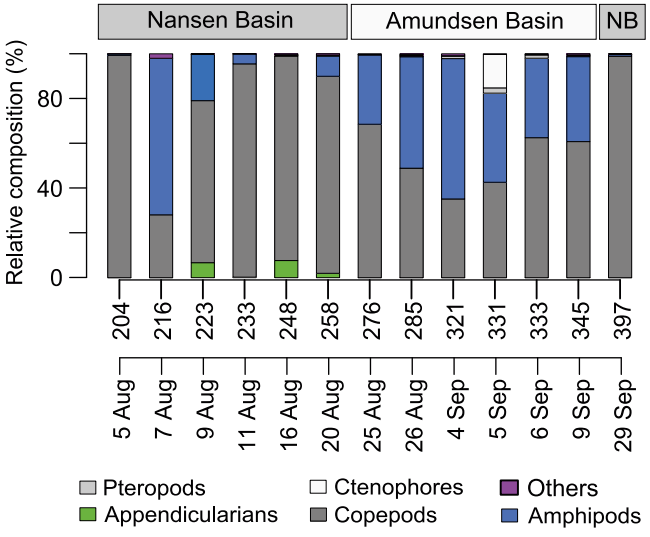

Fig. 4. Relative density of taxonomic groups at the sampling stations (numbers on the *x*-axis). NB: Nansen Basin

Table 3. List of species, with mean densities and frequency of occurrence over the sampling area. SD: standard deviation

Taxon	Mean density (ind. 100 m^{-2})	SD	Range	Frequency of occurrence
CTENOPHORA				
Beroe spp. Fabricius, 1780	2.11	4.75	0–15.79	0.85
Mertensia ovum Fabricius, 1780	0.19	0.38	0–1.35	0.85
MOLLUSCA				
Pteropoda				
Clione limacina Phipps, 1774	0.69	0.87	0–2.76	0.69
Limacina helicina Phipps, 1774	1.13	2.89	0–10.64	0.62
ANNELIDA				
Polychaeta				
Unidentified polychaete	<0.01	0.02		0.23
ARTHROPODA				
Crustacea				
Amphipoda				
Apherusa glacialis Hansen, 1888	58.19	70.48	0.33–221.84	1.00
Eusirus holmi Hansen, 1887	0.19	0.22	0–0.62	0.69
Gammaracanthus loricatus Sabine, 1821	<0.01	0.01	0–0.04	0.15
Gammarus wilkitzkii Birula, 1897	0.10	0.18	0–0.71	0.92
Onisimus glacialis Sars, 1900	1.12	1.34	0–3.97	0.85
Onisimus nanseni Sars, 1900	0.35	0.57	0–1.66	0.46
Themisto abyssorum Boeck, 1871	0.75	1.07	0–3.13	0.69
Themisto libellula Lichtenstein, 1822	20.14	25.69	0.11–85.36	1
Euphausiacea				
Thysanoessa inermis Kroyer, 1861	0.03	0.07	0–0.25	0.31
Unidentified euphausid	<0.01	0.01	0–0.04	0.08
Copepoda				
Calanus finmarchicus Gunnerus, 1765	52.40	187.39	0–676.04	0.23
Calanus glacialis Jaschnov, 1955	641.27	1078.52	3.78–3052.83	1
Calanus hyperboreus Kroyer, 1838	104.08	174.46	0–494.62	0.85
Pseudocalanus spp. Boeck, 1872[a]	24.60	33.29	0–109.22	0.92
Metridia longa Lubbock, 1854	172.47	619.49	0–2234.26	0.31
Paraeuchaeta glacialis Hansen, 1886	0.08	0.17	0–0.44	0.23
Unidentified harpacticoid[a]	0.32	0.69	0–1.96	0.31
Tisbe spp.[a]	20.13	20.26	0–68.26	0.92
Ostracoda				
Boroecia borealis Sars, 1866	<0.01	0.01	0–0.04	0.08
CHAETOGNATHA				
Eukrohnia hamata Möbius, 1875	11.01	36.3	0–131.76	0.69
Parasagitta elegans Verrill, 1873	0.15	0.28	0–1.01	0.54
CHORDATA				
Appendicularia				
Oikopleura vanhoeffeni Lohmann, 1896	47.37	145.39	0–526.54	0.31
VERTEBRATA				
Osteichthyes				
Boreogadus saida Lepechin, 1774	0.41	0.42	0–1.2	0.77

[a]Values might be underestimated due to small size of the organisms relative to the mesh size used

Cumulated densities of all species ranged from 0.3 ind. m^{-2} at Stn 216 to 69 ind. m^{-2} at Stn 248 (Fig. 5). Overall densities were significantly higher in the Nansen Basin regime than in the Amundsen Basin regime (W = 6, p-value < 0.05) (Fig. 5). This difference between the 2 environmental regimes remained relevant even when Stn 248, which had the highest abundance, was excluded from statistical analysis (W = 6, p-value < 0.05). The most abundant species were the copepods *Calanus hyperboreus* and *C. glacialis*. The low density exception at Stn 216 was caused by exceptionally low numbers of copepods. Stn 248 was unique in its species composition. Only at this station did *C. finmarchichus* dominate numer-

Table 4. Diversity indices calculated at each sampling station

Station no.	Richness	Shannon	Evenness
204	8	0.04	0.02
216	13	1.30	0.51
223	17	1.68	0.59
233	13	0.74	0.29
248	19	1.21	0.41
258	19	1.16	0.40
276	18	1.61	0.56
285	20	1.43	0.48
321	16	1.78	0.64
331	19	2.02	0.69
333	18	1.52	0.53
345	18	1.76	0.61
397	17	0.45	0.16
Nansen Basin	24	0.94	0.34
Amundsen Basin	24	1.69	0.58
Total	28	1.28	0.45

ically, and high densities of the appendicularian *Oikopleura vanhoeffeni* and the chaetognats *Eukrohnia hamata* and *Parasagitta elegans* were encountered. The biomass composition at this station was heavily dominated by ctenophores and tunicates. The last station (Stn 397) in the Nansen Basin regime differed from all other stations by a dominance of *Metridia longa* over all other copepod species. Among the amphipods, the ice-associated species *Apherusa glacialis* was numerically dominant at all stations, except the 2 open-water stations (Stns 331 and 333) in the Amundsen Basin. Here, the amphipod *Themisto libellula* was most abundant, though also present throughout the sampling area. Polar cod was present over the survey area with few exceptions: the open-water, slope station (Stn 204), a station (Stn 233) at which technical trawling problems probably affected the catch efficiency of the net for fast-swimming fish, and the early winter station (Stn 397). The density of polar cod ranged from 0.3 to 1.2 ind. 100 m^{-2}, with highest densities at Stns 285 and 345 in the Amundsen Basin regime. In contrast to nearby under-ice stations, polar cod densities at the 2 open-water stations in the Amundsen Basin (Stns 331 and 333) were close to zero.

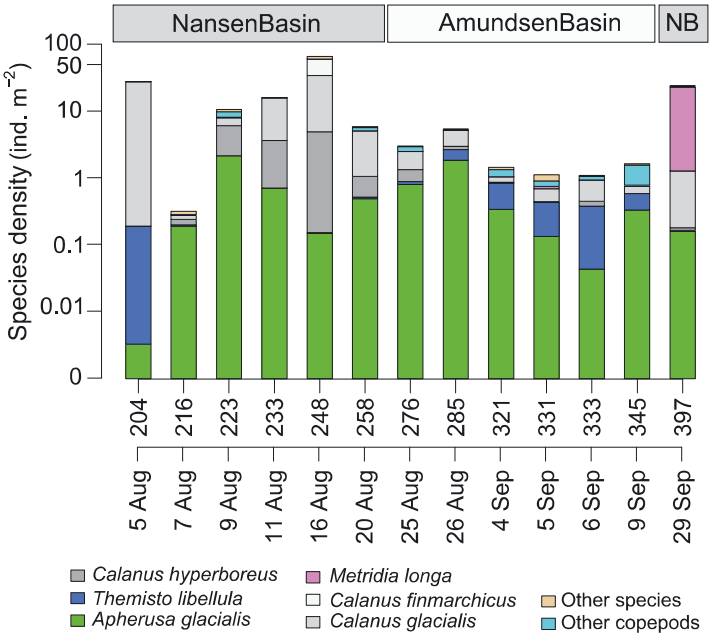

Fig. 5. Species' cumulated density at the sampling stations (numbers on the *x*-axis). Densities are shown in log scale. Only dominant taxa are represented in the legend. NB: Nansen Basin

The association of environment and biota

The NMDS ordination of the community resembled the gradients of environmental variables of the PCA. In the NMDS ordination, stations grouped mainly according to the 2 environmental regimes of the

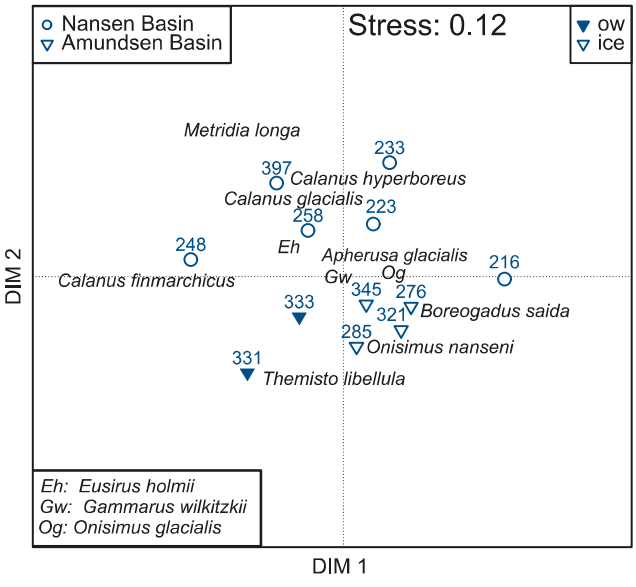

Fig. 6. Non-parametric multi-dimensional scaling (NMDS) plot of the under-ice community structure. Station symbols (circles: Nansen Basin; triangles: Amundsen Basin; ow: open water; ice: under-ice) indicate the relative position of the community composition at each sampling location in the NMDS ordination. Species names indicate the relative position of polar cod and numerically dominant species in the NMDS ordination. DIM 1 & 2: NMDS dimension axes

Nansen and Amundsen Basins (ANOSIM: R = 0.38, p-value = 0.016) (Fig. 6). The copepods *C. hyperboreus* and *C. glacialis* and the amphipod *Eusirus holmii* were associated with the Nansen Basin regime. Polar cod and the amphipods *Onisimus nanseni* and *T. libellula* were associated with the Amundsen Basin regime. Stn 216 in the Nansen Basin grouped closer to the Amundsen Basin regime due to its high density of polar cod and *O. nanseni* and low copepod density. The amphipods *A. glacialis*, *G. wilkitzkii* and *Onisimus glacialis* grouped in the centre of the NMDS plot, indicating equal association with Nansen Basin regime and Amundsen Basin regime stations. The stations from the Amundsen Basin regime were more homogenous, presenting smaller distances between stations' positions in the NMDS ordination than those in the Nansen Basin regime. The 2 open-water stations, however, grouped clearly apart from the other stations in the Amundsen Basin regime. They were associated with the pelagic amphipod *T. libellula.*

The Mantel test and BioEnv analysis both showed a strong positive correlation between the environmental and biological datasets (Mantel test: Pearson correlation coefficient = 0.65, $p < 0.001$). In the BioEnv, nitrate + nitrite concentration in the surface layer had the highest correlation of a single environmental variable (0.60) with the variability of density-based species distribution (Table 5). The highest correlation (0.75) with the variability of density-based species distribution was achieved by a combination of nitrate + nitrite concentration, surface-water temperature and salinity, ice thickness, mixed-layer depth and surface chlorophyll *a* concentration (Table 5).

DISCUSSION

Under-ice habitat properties

During summer 2012 the Arctic Ocean experienced a historical minimum sea-ice extent (Parkinson & Comiso 2013). Polarstern cruise ARK XXVII/3 sampled in the high central Arctic during that time, first across the Nansen Basin during early August, and then across the Amundsen Basin during late August–early September, almost reaching the North Pole at 87.87°N, 59.65°E. Daily sea-ice concentration data, from passive microwave satellite measurements, were >90% in the Nansen Basin during August and approximately 70% in the Amundsen Basin during September (data source: www.meereisportal.de; University of Bremen). These values were in good agreement with the range of sea-ice coverage determined from SUIT sensors. At only 1 station (Stn 216) did these observations differ from the SUIT sensor-derived ice coverage of 100%, whereas satellite-derived ice coverage was 40%, averaged over 350 km^2, placing this station in the marginal ice zone. Our sampling area was mainly covered with FYI (>95%), with only small fractions of MYI (Boetius et al. 2013). In our ice-thickness profiles, modal ice thicknesses ranged from 0.45 to 1.25 m. In general, modal ice thickness was higher and more variable in the Nansen Basin regime than in the Amundsen Basin regime. Modal ice thicknesses from our SUIT hauls resembled the general pattern of airborne ice thickness measurements carried out in the survey area during ARK XXVII/3 (Lange & Hendricks pers. comm.). Electromagnetic airborne sea-ice thickness

Table 5. Combinations of environmental variables selected by BioEnv analysis. Variables were ranked according to their correlation coefficients with the biological dataset. r: Spearman's correlation coefficient; other abbreviations as in Table 2

No. of variables	Environmental variables	r
1	NO_x	0.60
11	NO_x + Temperature + Salinity + Thickness + SD + Coverage + MLD + Chl*a*-surface + Chl*a* + Relative light + Si	0.67
2	NO_x + Temperature	0.69
3	NO_x + Temperature + Salinity	0.69
10	NO_x + Temperature + Salinity + Thickness + SD + MLD + Chl*a*-surface + Chl*a* + Relative light + Si	0.69
5	NO_x + Temperature + Salinity + Thickness + MLD	0.72
9	NO_x + Temperature + Salinity + Thickness + SD + MLD + Chl*a*-surface + Chl*a* + Relative light	0.72
4	NO_x + Temperature + Salinity + Thickness	0.73
6	NO_x + Temperature + Salinity + Thickness + Chl*a*-surface + Chl*a*	0.73
7	NO_x + Temperature + Salinity + Thickness + SD + MLD + Chl*a*	0.75
8	NO_x + Temperature + Salinity + Thickness + SD + MLD + Chl*a*-surface + Chl*a*	0.75

measurements confirm this range as mainly FYI (Haas et al. 2008). Therefore, our local sampling profiles largely resembled the general regional-scale situation in terms of sea-ice concentration, age class and thickness.

Apart from sea-ice properties, our PCA results indicated that a variety of other environmental parameters structured our sampling stations into 2 regimes, which were broadly coherent with the 2 ocean basins sampled. These differences could in part be explained by seasonal processes, such as the melting of sea ice or the deepening of the mixed layer in the Amundsen Basin in late summer. We acknowledge the difficulty of disentangling spatial from temporal trends over our sampling area. We sampled within the pack ice, first in the Nansen Basin during early August, when a more compact sea-ice cover was present. At the end of August, while sampling in the Amundsen Basin, the pack ice began to loosen and ice was thinning, leaving locally large open-water areas, for example at Stns 331 and 333. Therefore, gradients of sea-ice properties were highly associated with the seasonal progression towards the end of summer, until the minimum sea-ice extent occurred on 13 September (Parkinson & Comiso 2013). Break-up of sea ice by early September likely allowed more light to penetrate into the water column. This favoured the increased chlorophyll *a* concentration we observed in the Amundsen Basin regime, locally depleting nutrients in the surface layer. This was demonstrated by the association of the open-water stations with higher chlorophyll *a* concentrations (Fig. 2). Our last station sampled at the onset of winter in the Nansen Basin (Stn 397), however, had typical 'Nansen regime' values again, i.e. high salinity and low silicate concentrations at the depth of the chlorophyll *a* maximum (Fig. 2). This indicates that there was a strong regional component structuring the 2 regimes, besides some undoubtedly present seasonal trends.

The regional differences between the 2 regimes can largely be explained by water mass properties and circulation patterns. The Eurasian Basin is a permanently ice-covered basin with depths >4000 m. The Gackel Ridge subdivides this basin into the nearly equally sized Nansen and Amundsen Basins. The Transpolar Drift current crosses both basins, transporting Polar Surface Water and sea ice from the Siberian shelf through the central Arctic Ocean towards the Fram Strait. A portion of the sea-ice cover is recirculated within the anti-cyclonic Beaufort Gyre in the central and western Arctic Ocean, contributing to the formation of MYI (Rigor & Wallace 2004). A considerable portion of the marginal sea ice, however, is advected out of the Arctic Ocean through the Fram Strait (Kwok et al. 2004).

Nutrient-rich Atlantic Water is advected into the Eurasian Basin by 2 main branches: the Fram Strait branch and the Barents Sea branch. The Fram Strait branch of warm Atlantic Water is largely recirculated within the Nansen Basin, whereas the remaining Arctic Ocean basins, including the Amundsen Basin, are dominated by the Barents Sea branch (Rudels et al. 2013). This branch experiences water exchange by advection from the Laptev Sea continental margin, which is enriched in silicate (Bauch et al. 2014). Consequently, we found high silica and low nitrate + nitrite and phosphate concentrations in the Amundsen Basin regime and the opposite situation in the Nansen Basin regime. Generally, Eurasian Basin regions with higher salinity indicate a higher Atlantic influence and can have surface nitrate concentrations in excess of 5 µmol l^{-1} even in summer (Codispoti et al. 2013). During our sampling, high salinities, high nitrate + nitrite and high phosphate concentrations were present in the surface water of the Nansen Basin regime. Two stations, Stns 204 and 248, were exceptionally rich in nitrate + nitrite, with values at the chlorophyll maximum depth reaching up to 6.8 µmol l^{-1}. Stn 204 was situated on the Svalbard slope, near the inflow of Atlantic Water into the Arctic Ocean. Stn 248 was located near a convergent front formed by the Atlantic Water boundary current (Lalande et al. 2014). Nearby surface salinity and temperature profiles suggest freezing occurred prior to our arrival. The mixing due to haline convection during freezing could have added nutrients to the mixed layer from below, explaining the higher nitrate + nitrite and chlorophyll *a* concentrations.

Under-ice community composition

We identified a total of 28 species in the upper 2 m of the mostly ice-covered water column. In terms of species numbers, amphipods and copepods equally dominated the community with 8 species each (Table 3). Our overall species richness was low compared to previous, geographically more extended studies on Arctic epipelagic fauna (Kosobokova & Hirche 2000, Auel & Hagen 2002, Kosobokova & Hopcroft 2010, Kosobokova et al. 2011). Such comparisons are, however, complicated by differences in net type, mesh sizes and sampled depth interval. Most Arctic zooplankton studies integrated the epipelagic community over at least the upper 50 m.

The species composition from those studies is thus much more influenced by pelagic fauna, mostly dominated by the often deeper dwelling copepods (Kosobokova & Hirche 2000). Considering ice-associated species reported from the northern Barents Sea, Svalbard, Laptev Sea, or Greenland Sea (Werner & Arbizu 1999, Hop et al. 2000b, Werner & Gradinger 2002, Werner & Auel 2005), our study found the highest species richness compared to any individual study. This might be due to a larger under-ice surface area of approximately 4 km^2 sampled per station in our study. Sampling effort in previous under-ice studies was spatially limited to single ice floes and was mainly performed by divers with pumps or estimates made from video surveys (Werner & Gradinger 2002, Hop & Pavlova 2008, Hop et al. 2011). These studies described ice-associated species related to ice concentration and topography (Hop et al. 2000b, Werner & Gradinger 2002). But ice properties vary greatly from one ice floe to another, as does the ice-associated fauna. Using the SUIT enabled us to integrate both floes with low faunal densities and floes with high faunal densities. This approach can representatively capture the meso-scale variability of the under-ice environment and facilitate large-scale density estimates if other error sources are minimal. Such error sources may be the low efficiency of the SUIT to sample animals from crevices and wedges in the ice, or the ability of polar cod to avoid or escape the net. Reported habitat preferences and behaviour of the species sampled in this study indicate that underestimation due to preference of crevices may apply to single predatory species (e.g. *Gammarus wilkitzkii*), but not to those species clearly dominant in density in our and other under-ice studies, such as *Apherusa glacialis* or *Onisimus glacialis* (Gradinger & Bluhm 2004, Hop & Pavlova 2008, Gradinger et al. 2010). Videos from the SUIT camera show no indication of escape or avoidance of the net by polar cod, but the loss of fish through behavioural response cannot be assessed with certainty. The omnipresence of polar cod in under-ice catches rather indicated that the sluggish lifestyle of this species (Gradinger & Bluhm 2004) may have worked in favour of sampling this species with a net that is relatively ineffective for catching fast-swimming fish.

We found higher densities of under-ice fauna in the Nansen Basin regime than in the Amundsen Basin regime. This pattern was mainly driven by high densities of large calanoid copepods. In the central Arctic Ocean, the mesozooplankton community in the surface 50 m is known to be dominated by *Calanus* spp. (Auel & Hagen 2002). The big herbivorous *C. hyperboreus* and *C. glacialis* dominated in our samples, contributing on average 9 and 38%, respectively, to the total density of the surface-layer community. *C. glacialis* largely dominated the surface community at the slope station (Stn 204), with 99%. The Atlantic water species *C. finmarchichus* appeared in high numbers at only 1 station in the Nansen Basin (Stn 248). Situated near a convergence front, a freezing event prior to our arrival is believed to have caused convective mixing and entrainment of nutrients from the subsurface Atlantic Water at that station (Lalande et al. 2014). More nutrients added to the euphotic layer could have favoured increased productivity and subsequent immigration of grazers from the deeper Atlantic Water layer.

Besides the 3 *Calanus* species, *Metridia longa* and the smaller copepods *Pseudocalanus* spp. are important contributors to the surface community, in both the eastern (Kosobokova et al. 2011) and the western Arctic Ocean (Matsuno et al. 2012). A switch in dominance occurred at our last station, at the onset of freezing. Coincident with the migration of *Calanus* spp. into deeper layers (Hirche 1997, Fortier et al. 2001, Madsen et al. 2001, Darnis & Fortier 2014), *M. longa* largely dominated the surface community (Fig. 5). This species is known to remain active year-round (Ashjian et al. 2003), but seldom occurs above depths <25 m (Fortier et al. 2001). Low competition, avoidance of visual predators and food availability at the ice underside might explain their rise to the ice–water interface at Stn 397. Also active year-round are the small copepods of the genus *Pseudocalanus* (Fortier et al. 2001). They were widespread across the 2 basins without any seasonal or regional patterns. The year-round active copepods might represent a nutritious food source for polar cod and other predatory members of the under-ice community during Arctic winter.

Six species of ice-associated amphipods were found in our study area. Our results are in agreement with numerous under-ice studies in finding that *A. glacialis* dominates the ice-amphipod community in FYI-dominated environments (Werner & Auel 2005). Where MYI and ridges are more prevalent, *Gammarus wilkitzkii* occurs in higher abundances (Lønne & Gulliksen 1991, Beuchel & Lønne 2002). Whereas *A. glacialis* is found mainly in the water just below the ice, *G. wilkitzkii* stays mainly attached to the under-side of ice and hides in ice cracks (Hop et al. 2000b, Hop & Pavlova 2008). We found only few *G. wilkitzkii* individuals at each station, but consistently over both basins. Ice thickness was highly variable, with ridges at all ice-covered stations, even though

we sampled mainly under FYI. Interestingly, we found young *G. wilkitzkii* juveniles just released from the brood pouch in September, whereas the release period was previously documented to occur between April and May in the northern Barents Sea (Poltermann et al. 2000). One female of the rare ice-amphipod *Gammaracanthus loricatus* and a few *Onisimus* spp. females were also observed carrying juveniles in their pouches. Such a difference in the timing of juvenile release could be related to sea-ice seasonal dynamics and consequently food availability. Near Svalbard and in the Barents Sea, ice melting starts earlier. The spring bloom usually occurs in April, followed by high abundances of *Calanus* spp. This spring to summer succession in the food chain is regarded as an important factor for releasing the amphipods' young (Dalpadado 2002).

Swarms of the pelagic amphipod *Themisto libellula* have been reported to rise under landfast-ice (Gulliksen 1984). We noticed high numbers of *T. libellula* juveniles under the ice in the Amundsen Basin regime. At 2 locations, we observed a distinct change in community structure between nearby open-water and under-ice sampling locations. The difference in ice coverage was accurately mirrored by a clear dominance of the ice-associated amphipod *A. glacialis* in ice-covered waters versus a dominance of the pelagic amphipod *T. libellula* in the surface community of ice-free waters. This pattern suggests that habitat partitioning between sympagic and pelagic species is abrupt, creating a small-scale pattern in the surface-layer community according to ice conditions.

Two environmental regimes

In terms of species' presence, we found similar under-ice community compositions in the Nansen Basin and Amundsen Basin regimes. When the relative community structure was considered, however, gradual changes in community composition were ordered according to the 2 environmental regimes (Fig. 6). The Nansen regime was characterised by heavier sea ice, which can be considered as a compact, stable habitat. Both ice thickness and its standard deviation (an expression of sea-ice underside roughness) were correlated with the under-ice community structure. Around Svalbard, ice thickness was found to be the key variable impacting ice-associated faunal variability (Hop & Pavlova 2008).

Copepods (*Calanus* spp.) and the large ice-associated amphipod *E. holmii* were associated with the Nansen Basin regime (Fig. 6). In the water column, low chlorophyll *a* concentrations under a compact ice cover may indicate limited food availability due to light limitation, attracting copepods capable of under-ice grazing to the ice–water interface layer (Runge & Ingram 1991). In the more open Amundsen Basin regime, under-ice feeding was probably less important for *Calanus* spp., causing them to disperse in the water column. The Amundsen Basin was sampled 2 wk after the Nansen Basin and was characterised by autumn conditions with loose sea-ice coverage, indicating a decaying sea-ice habitat with low nutrient concentrations but with higher chlorophyll *a* concentrations in the water column. Under-ice faunal densities in the Amundsen Basin regime were lower, but had higher diversity than in the Nansen Basin regime (Table 4). The density of adult copepods in the surface layer was considerably lower than in the Nansen Basin regime. There were, however, high numbers of *Calanus* spp., stages CI to CIII, present. These stages were not included in our density calculations, because the numbers caught did not represent true abundances due to our 0.3 mm mesh zooplankton net. These findings agree with the general patterns of seasonal vertical migration of *Calanus* spp. (Darnis & Fortier 2014). Migration of *Calanus* spp. starts in August in the Amundsen Gulf (Beauford Sea) (Darnis & Fortier 2014) and Fram Strait (Auel et al. 2003). At the end of summer, most copepods and their smaller stages have stored lipids, accounting for up to 50% of their body weight (Scott et al. 1999), to prepare for diapause (Auel et al. 2003). Only juvenile stages CI to CIII of *C. hyperboreus* were noted to remain in the surface layer (Darnis & Fortier 2014). The progressive reduction of copepod numbers in our samples suggests that emigration from the surface layer might have gradually started at the end of August. With the decreased copepod density in the Amundsen Basin regime, the amphipods numerically co-dominated the under-ice community. Particularly, the carnivorous amphipod *T. libellula* was more abundant in the Amundsen Basin regime than in the Nansen Basin regime (Fig. 5). As a preferred prey of *T. libellula* (Auel et al. 2002, Noyon et al. 2009), the small copepodites could have attracted *T. libellula* to the surface layer. Overall, the Amundsen Basin regime appeared to support more carnivorous fauna, with a higher proportion of larger animals, such as *T. libellula*, *O. nanseni* and polar cod. Higher sinking fluxes of detritus in the Amundsen Basin caused by melting sea ice (Lalande et al. 2014) indicate that additional

food became available in the ice-water interface layer for opportunistic feeders, such as the amphipods *O. glacialis*, *O. nanseni* and *G. wilkitzkii* (Werner 1997).

A high degree of heterotrophy in the food web is supported for the entire Eurasian Basin by a tentative comparison of primary production versus food demand of the dominant grazers during our sampling period. In ice-covered waters of the Eurasian Basin, the integrated (median) primary production rate measured at the time of our sampling was 0.7 mg C m^{-2} d^{-1} in sea ice and 18 mg C m^{-2} d^{-1} in the water column (Fernández-Méndez 2014). Experimentally derived mean ingestion rates range between 2.8 and 8.4 µg C $ind.^{-1}$ d^{-1} for *C. hyperboreus* and between 6.0 and 18.0 µg C $ind.^{-1}$ d^{-1} for *C. glacialis* (Olli et al. 2007). For the herbivorous amphipod *A. glacialis*, the mean ingestion rate is about 13 µg C $ind.^{-1}$ d^{-1} (Werner 1997). Based on the mean densities of these species found in the ice–water interface layer (Table 3), their cumulative mean carbon demand ranged from about 0.1 to 0.2 mg C m^{-2} d^{-1}. Only a fraction of the carbon produced by ice algae, however, is available for grazers at the ice underside. This implies that the production of ice algae could have barely matched the food demand of under-ice grazers during the sampling period. Locally, however, they may have benefited from feeding on biomass-rich algal aggregates floating under the sea ice (Fernández-Méndez et al. 2014). In the water column, 0–200 m integrated densities of *C. hyperboreus* and *C. glacialis* derived from multinet sampling during the same cruise (B. Niehoff & J. Ehrlich unpubl. data) imply a mean carbon demand range of 9.5 to 28.4 mg C m^{-2} d^{-1} based on the copepod ingestion rates according to Olli et al. (2007). In sea ice and the water column combined, a nearly 1:1 ratio of primary production versus grazer food demand could have contributed significantly to the low overall chlorophyll *a* concentrations in sea ice and water during our sampling period. It further indicates that peak production levels generating zooplankton growth had passed at most sampling locations before our sampling. This scenario agrees well with the mass export of algal biomass to the sea floor observed by Boetius et al. (2013) at several ice-sampling stations during our cruise, suggesting a major production peak in the investigation area prior to our sampling. At the time of sampling, the increased populations of zooplankton and under-ice fauna resulting from this bloom relied more on heterotrophic carbon sources than on autotrophic production.

CONCLUSIONS

This first large-scale survey of under-ice fauna in the Arctic deep-sea shows that a variety of species, including amphipods and polar cod, are present virtually everywhere in the Eurasian Basin, in spite of its presumed low productivity. Although under-ice faunal densities were relatively low compared to sea-ice habitats on the shelf, the omnipresence of animals in the vast deep-sea basins highlights the large-scale importance of the under-ice habitat in the Arctic Ocean.

Differences in sea-ice properties and nutrient concentrations were the key factors separating the sampled environments into the Nansen and Amundsen Basin regimes. The separation of these 2 regimes had both a seasonal and a strong regional component related to water-mass distribution, ice drift and current patterns. The under-ice community structure followed this environmental gradient, indicating a decisive role of both sea-ice and water-column characteristics for the distribution of species in the surface layer. Abrupt changes in the dominance of ice-associated amphipods at ice-covered stations versus pelagic amphipods at nearby ice-free stations emphasised a distinct influence of sea ice on small-scale patterns in the surface-layer community.

With respect to the decades of sea-ice decline before 2012, it is likely that the situation encountered in our study reflected a snapshot of a system in transition. Whether the past central Arctic under-ice community was more or less abundant, or differed in diversity and composition, is impossible to assess in the absence of appropriate baseline data. In the future, the central Arctic under-ice community will be exposed to continuing changes, including a further shortening of the ice-covered season, the complete disappearance of multi-year ice and changes in stratification and nutrient regimes. Due to their position around the North Pole, the central Arctic basins may constitute a critical refuge for the specifically ice-adapted biota of the Arctic Ocean for several decades. Whether or not the central Arctic Ocean can fulfil this function will depend on the many direct and indirect changes affecting the Arctic pack-ice and the resilience of individual ice-associated species. The subtle response of the under-ice community to many of these changing parameters suggests that changes already have impacted Arctic under-ice communities and will continue to do so in the future. Monitoring the course of changes in Arctic biodiversity and ecosystem structure will be key requirements for successful resource and conservation management in an Arctic Ocean in transition.

Acknowledgements. We thank Captain Uwe Pahl and the crew of the RV 'Polarstern' expedition IceArc (ARK XXVII/3) for their excellent support with work at sea. We thank Jan Andries van Franeker (IMARES) for kindly providing the surface and under-ice trawl (SUIT) and Michiel van Dorssen for technical support with work at sea. We thank Karel Bakker for kindly providing the nutrient data. We thank Ilka Peeken for chlorophyll *a* measurements used for the calibration of under-ice fluorescence data. SUIT was developed by IMARES with support from the Netherlands Ministry of EZ (Project WOT-04-009-036) and the Netherlands Polar Program (Project ALW 866.13.009). This study is part of the Helmholtz Association Young Investigators Group *Iceflux*: ice-ecosystem carbon flux in polar oceans (VH-NG-800). We thank the 3 anonymous reviewers for their helpful suggestions and comments that contributed significantly to the improvement of the manuscript.

LITERATURE CITED

Arctic Climate Impact Assessment A (2004) Impacts of a warming Arctic. Cambridge University Press, Cambridge

Arndt CE, Pavlova O (2005) Origin and fate of ice fauna in the Fram Strait and Svalbard area. Mar Ecol Prog Ser 301:55–66

Arrigo KR, van Dijken GL (2011) Secular trends in Arctic Ocean net primary production. J Geophys Res Oceans 116:C09011, doi:10.1029/2011CJ007151

Arrigo KR, van Dijken G, Pabi S (2008) Impact of a shrinking Arctic ice cover on marine primary production. Geophys Res Lett 35:19603, doi:10.1029/2008GL035028

Ashjian CJ, Campbell RG, Welch HE, Butler M, Van Keuren D (2003) Annual cycle in abundance, distribution, and size in relation to hydrography of important copepod species in the western Arctic Ocean. Deep-Sea Res I 50: 1235–1261

Auel H, Hagen W (2002) Mesozooplankton community structure, abundance and biomass in the central Arctic Ocean. Mar Biol 140:1013–1021

Auel H, Harjes M, da Rocha R, Stübing D, Hagen W (2002) Lipid biomarkers indicate different ecological niches and trophic relationships of the Arctic hyperiid amphipods *Themisto abyssorum* and *T. libellula.* Polar Biol 25: 374–383

Auel H, Klages M, Werner I (2003) Respiration and lipid content of the Arctic copepod *Calanus hyperboreus* overwintering 1 m above the seafloor at 2,300 m water depth in the Fram Strait. Mar Biol 143:275–282

Bauch D, Torres-Valdes S, Polyakov I, Novikhin A, Dmitrenko I, McKay J, Mix A (2014) Halocline water modification and along slope advection at the Laptev Sea continental margin. Ocean Science 10:141–154

Benoit D, Simard Y, Gagné J, Geoffroy M, Fortier L (2010) From polar night to midnight sun: photoperiod, seal predation, and the diel vertical migrations of polar cod (*Boreogadus saida*) under landfast ice in the Arctic Ocean. Polar Biol 33:1505–1520

Beuchel F, Lønne OJ (2002) Population dynamics of the sympagic amphipods *Gammarus wilkitzkii* and *Apherusa glacialis* in sea ice north of Svalbard. Polar Biol 25: 241–250

Boetius A, Albrecht S, Bakker K, Bienhold C and others (2013) Export of algal biomass from the melting Arctic sea ice. Science 339:1430–1432

Bradstreet MSW, Cross WE (1982) Trophic relationships at high Arctic ice edges. Arctic 35:1–12

Bray JR, Curtis JT (1957) An ordination of the upland forest communities of southern Wisconsin. Ecol Monogr 27: 325–349

Budge SM, Wooller MJ, Springer AM, Iverson SJ, McRoy CP, Divoky GJ (2008) Tracing carbon flow in an arctic marine food web using fatty acid–stable isotope analysis. Oecologia 157:117–129

Clarke KR (1993) Non-parametric multivariate analyses of changes in community structure. Aust J Ecol 18:117–143

Clarke K, Ainsworth M (1993) A method of linking multivariate community structure to environmental variables. Mar Ecol Prog Ser 92:205–219

Codispoti LA, Kelly V, Thessen A, Matrai P and others (2013) Synthesis of primary production in the Arctic Ocean. III. Nitrate and phosphate based estimates of net community production. Prog Oceanogr 110:126–150

Dalpadado P (2002) Inter-specific variations in distribution, abundance and possible life-cycle patterns of *Themisto* spp. (Amphipoda) in the Barents Sea. Polar Biol 25: 656–666

Darnis G, Fortier L (2014) Temperature, food and the seasonal vertical migration of key arctic copepods in the thermally stratified Amundsen Gulf (Beaufort Sea, Arctic Ocean). J Plankton Res 36:1092–1108

Falk-Petersen S, Mayzaud P, Kattner G, Sargent J (2009) Lipids and life strategy of Arctic *Calanus*. Mar Biol Res 5: 18–39

Fernández-Méndez M (2014) Primary productivity in Arctic sea ice and ocean. PhD dissertation, University of Bremen, Bremen

Fernández-Méndez M, Wenzhöfer F, Peeken I, Sørensen HL, Glud RN, Boetius A (2014) Composition, buoyancy regulation and fate of ice algal aggregates in the Central Arctic Ocean. PLoS ONE 9:e107452

Fetterer F, Knowles K, Meier W, Savoie M (2002) Sea ice index. Monthly mean sea ice extent. National Snow and Ice Data, Boulder, CO

Finley KJ, Gibb EJ (1982) Summer diet of the narwhal (*Monodon monoceros*) in Pond Inlet, northern Baffin Island. Can J Zool 60:3353–3363

Flores H, van Franeker J-A, Cisewski B, Leach H and others (2011) Macrofauna under sea ice and in the open surface layer of the Lazarev Sea, Southern Ocean. Deep-Sea Res II 58:1948–1961

Flores H, van Franeker JA, Siegel V, Haraldsson M and others (2012) The association of Antarctic krill *Euphausia superba* with the under-ice habitat. PLoS ONE 7:e31775

Fofonoff N (1985) Physical properties of seawater: a new salinity scale and equation of state for seawater. J Geophys Res Oceans 90:3332–3342

Fortier M, Fortier L, Hattori H, Saito H, Legendre L (2001) Visual predators and the diel vertical migration of copepods under Arctic sea ice during the midnight sun. J Plankton Res 23:1263–1278

Gosselin M, Levasseur M, Wheeler PA, Horner RA, Booth BC (1997) New measurements of phytoplankton and ice algal production in the Arctic Ocean. Deep-Sea Res II 44: 1623

Gradinger RR, Bluhm BA (2004) *In-situ* observations on the distribution and behavior of amphipods and Arctic cod (*Boreogadus saida*) under the sea ice of the High Arctic Canada Basin. Polar Biol 27:595–603

Gradinger R, Bluhm B, Iken K (2010) Arctic sea-ice ridges—safe heavens for sea-ice fauna during periods of extreme ice melt? Deep-Sea Res II 57:86–95

Gulliksen B (1984) Under-ice fauna from Svalbard waters. Sarsia 69:17–23

Haas C, Pfaffling A, Hendricks S, Rabenstein L, Etienne JL, Rigor I (2008) Reduced ice thickness in Arctic Transpolar Drift favors rapid ice retreat. Geophys Res Lett 35: L17501, doi:10.1029/2008GL034457

Harter BB, Elliott KH, Divoky GJ, Davoren GK (2013) Arctic cod (*Boreogadus saida*) as prey: fish length–energetics relationships in the Beaufort Sea and Hudson Bay. Arctic 66:191–196

Hirche HJ (1997) Life cycle of the copepod *Calanus hyperboreus* in the Greenland Sea. Mar Biol 128:607–618

Hop H, Gjøsæter H (2013) Polar cod (*Boreogadus saida*) and capelin (*Mallotus villosus*) as key species in marine food webs of the Arctic and the Barents Sea. Mar Biol Res 9: 878–894

Hop H, Pavlova O (2008) Distribution and biomass transport of ice amphipods in drifting sea ice around Svalbard. Deep-Sea Res II 55:2292–2307

Hop H, Poltermann M, Lonne OJ, Falk-Petersen S, Korsnes R, Budgell WP (2000a) Ice amphipod distribution relative to ice density and under-ice topography in the northern Barents Sea. Polar Biol 23:357–367

Hop H, Poltermann M, Lønne OJ, Falk-Petersen S, Korsnes R, Budgell WP (2000b) Ice amphipod distribution relative to ice density and under-ice topography in the northern Barents Sea. Polar Biol 23:357–367

Hop H, Mundy C, Gosselin M, Rossnagel A, Barber D (2011) Zooplankton boom and ice amphipod bust below melting sea ice in the Amundsen Gulf, Arctic Canada. Polar Biol 34:1947–1958

Hopcroft RR, Clarke C, Nelson RJ, Raskoff KA (2005) Zooplankton communities of the Arctic's Canada Basin: the contribution by smaller taxa. Polar Biol 28:198–206

Hunt BPV, Nelson RJ, Williams B, McLaughlin FA and others (2014) Zooplankton community structure and dynamics in the Arctic Canada Basin during a period of intense environmental change (2004 to 2009). J Geophys Res Oceans 119:2518–2538

Johannessen OM, Bengtsson L, Miles MW, Kuzmina SI and others (2004) Arctic climate change: observed and modelled temperature and sea-ice variability. Tellus Ser A Dyn Meteorol Oceanogr 56:328–341

Kosobokova K, Hirche HJ (2000) Zooplankton distribution across the Lomonosov Ridge, Arctic Ocean: species inventory, biomass and vertical structure. Deep-Sea Res I 47:2029–2060

Kosobokova K, Hirche HJ (2009) Biomass of zooplankton in the eastern Arctic Ocean—a base line study. Prog Oceanogr 82:265–280

Kosobokova KN, Hopcroft RR (2010) Diversity and vertical distribution of mesozooplankton in the Arctic's Canada Basin. Deep-Sea Res II 57:96–110

Kosobokova K, Hopcroft R, Hirche HJ (2011) Patterns of zooplankton diversity through the depths of the Arctic's central basins. Mar Biodiv 41:29–50

Kruskal JB (1964) Nonmetric multidimensional scaling: a numerical method. Psychometrika 29:115–129

Kwok R, Rothrock DA (2009) Decline in Arctic sea ice thickness from submarine and ICESat records: 1958–2008. Geophys Res Lett 36:L15501, doi:10.1029/2009GL039035

Kwok R, Cunningham GF, Pang SS (2004) Fram Strait sea ice outflow. J Geophys Res Oceans 109:C01009, doi:10.1029/2003JC001785

Laidre KL, Heide-Jørgensen MP (2005) Arctic sea ice trends and narwhal vulnerability. Biol Conserv 121:509–517

Lalande C, Nöthig EM, Somavilla R, Bauerfeind E, Shevchenko V, Okolodkov Y (2014) Variability in under-ice export fluxes of biogenic matter in the Arctic Ocean. Global Biogeochem Cycles 28:571–583

Legendre P, Legendre L (2012) Numerical ecology. Elsevier, Amsterdam

Lønne OJ, Gulliksen B (1991) Sympagic macro-fauna from multiyear sea-ice near Svalbard. Polar Biol 11:471–477

Madsen SD, Nielsen TG, Hansen BW (2001) Annual population development and production by *Calanus finmarchicus*, *C. glacialis* and *C. hyperboreus* in Disko Bay, western Greenland. Mar Biol 139:75–93

Mann HB, Whitney DR (1947) On a test of whether one of two random variables is stochastically larger than the other. Ann Math Stat 18:50–60

Mantel N (1967) The detection of disease clustering and a generalized regression approach. Cancer Res 27: 209–220

Mardia KV, Kent J, Bibby J (1979) Multivariate analysis (probability and mathematical statistics). Academic Press, London

Markus T, Stroeve JC, Miller J (2009) Recent changes in Arctic sea ice melt onset, freezeup, and melt season length. J Geophys Res Oceans 114:C12024, doi:10.1029/2009JC005436

Maslanik J, Stroeve J, Fowler C, Emery W (2011) Distribution and trends in Arctic sea ice age through spring 2011. Geophys Res Lett 38:L13502, doi:10.1029/2011GL047735

Matley J, Fisk A, Dick T (2013) The foraging ecology of Arctic cod (*Boreogadus saida*) during open water (July–August) in Allen Bay, Arctic Canada. Mar Biol 160: 2993–3004

Matsuno K, Yamaguchi A, Shimada K, Imai I (2012) Horizontal distribution of calanoid copepods in the western Arctic Ocean during the summer of 2008. Polar Sci 6: 105–119

Mehlum F, Gabrielsen GW (1993) The diet of high-Arctic seabirds in coastal and ice-covered, pelagic areas near the Svalbard archipelago. Polar Res 12:1–20

Melnikov I, Kulikov A (1980) The cryopelagic fauna of the central Arctic basin. Biology of the central Arctic Basin. Nauka, Moscow, p 97–111

Minchin PR (1987) An evaluation of the relative robustness of techniques for ecological ordination. In: Prentice IC, van der Maarel E (eds) Theory and models in vegetation science. Springer, Heidelberg, p 89–107

Motoda S (1959) Devices of simple plankton apparatus. Mem Fac Fish Hokkaido Univ 7:73–94

Noyon M, Gasparini S, Mayzaud P (2009) Feeding of *Themisto libellula* (Amphipoda Crustacea) on natural copepods assemblages in an Arctic fjord (Kongsfjorden, Svalbard). Polar Biol 32:1559–1570

Olli K, Wassmann P, Reigstad M, Ratkova TN and others (2007) The fate of production in the central Arctic Ocean—top-down regulation by zooplankton expatriates? Prog Oceanogr 72:84–113

Overland JE, Wang M (2013) When will the summer Arctic be nearly sea ice free? Geophys Res Lett 40:2097–2101

Parkinson CL, Comiso JC (2013) On the 2012 record low Arctic sea ice cover: combined impact of preconditioning and an August storm. Geophys Res Lett 40:1356–1361

Poltermann M, Hop H, Falk-Petersen S (2000) Life under Arctic sea ice — reproduction strategies of two sympagic (ice-associated) amphipod species, *Gammarus wilkitzkii* and *Apherusa glacialis.* Mar Biol 136:913–920

Polyakov IV, Beszczynska A, Carmack EC, Dmitrenko IA and others (2005) One more step toward a warmer Arctic. Geophys Res Lett 32:L17605, doi:10.1029/2005GL023740

Pomerleau C, Nelson RJ, Hunt BPV, Sastri AR, Williams WJ (2014) Spatial patterns in zooplankton communities and stable isotope ratios ($\delta^{13}C$ and $\delta^{15}N$) in relation to oceanographic conditions in the sub-Arctic Pacific and western Arctic regions during the summer of 2008. J Plankton Res 36:757–775

R Core Team (2012) R: a language and environment for statistical computing. R Foundation for Statistical Computing, Vienna. www.R-project.org

Rabe B, Wisotzki A, Rettig S, Somavilla Cabrillo R, Sander H (2012) Physical oceanography during POLARSTERN cruise ARK-XXVII/3 (IceArc) PANGEA. Alfred Wegener Institute, Helmholtz Center for Polar and Marine Research, Bremerhaven

Rigor IG, Wallace JM (2004) Variations in the age of Arctic sea-ice and summer sea-ice extent. Geophys Res Lett 31:L09401, doi:10.1029/2004GL019492

Rudels B, Schauer U, Björk G, Korhonen M, Pisarev S, Rabe B, Wisotzki A (2013) Observations of water masses and circulation in the Eurasian Basin of the Arctic Ocean from the 1990s to the late 2000s. Ocean Sci 9:147–169

Runge JA, Ingram RG (1991) Under-ice feeding and diel migration by the planktonic copepods *Calanus glacialis* and *Pseudocalanus minutus* in relation to the ice algal production cycle in southeastern Hudson Bay, Canada. Mar Biol 108:217–225

Scott CL, Falk-Petersen S, Sargent JR, Hop H, Lønne OJ, Poltermann M (1999) Lipids and trophic interactions of ice fauna and pelagic zooplankton in the marginal ice zone of the Barents Sea. Polar Biol 21:65–70

Shannon C (1948) A mathematical theory of communication. Bell Syst Tech J 27:379–423

Shaw WJ, Stanton TP, McPhee MG, Morison JH, Martinson DG (2009) Role of the upper ocean in the energy budget of Arctic sea ice during SHEBA. J Geophys Res Oceans 114:C06012, doi:10.1029/2008JC004991

Shimada K, Kamoshida T, Itoh M, Nishino S and others (2006) Pacific Ocean inflow: influence on catastrophic reduction of sea ice cover in the Arctic Ocean. Geophys Res Lett 33:L08605, doi:10.1029/2005GL025624

Smouse PE, Long JC, Sokal RR (1986) Multiple regression and correlation extensions of the Mantel test of matrix correspondence. Syst Zool 35:627–632

Søreide JE, Hop H, Carroll ML, Falk-Petersen S, Hegseth EN (2006) Seasonal food web structures and sympagic–pelagic coupling in the European Arctic revealed by stable isotopes and a two-source food web model. Prog Oceanogr 71:59–87

Søreide JE, Carroll ML, Hop H, Ambrose WG, Hegseth EN, Falk-Petersen S (2013) Sympagic-pelagic-benthic coupling in Arctic and Atlantic waters around Svalbard revealed by stable isotopic and fatty acid tracers. Mar Biol Res 9:831–850

Spreen G, Kaleschke L, Heygster G (2008) Sea ice remote sensing using AMSR-E 89-GHz channels. J Geophys Res Oceans 113:C02S03

Stroeve J, Holland MM, Meier W, Scambos T, Serreze M (2007) Arctic sea ice decline: faster than forecast. Geophys Res Lett 34:L09501, doi:10.1029/2007GL029703

Stroeve J, Serreze M, Holland M, Kay J, Malanik J, Barrett A (2012) The Arctic's rapidly shrinking sea ice cover: a research synthesis. Clim Change 110:1005–1027

Tremblay JÉ, Gagnon J (2009) The effects of irradiance and nutrient supply on the productivity of Arctic waters: a perspective on climate change. In: Nihoul JJ, Kostianoy A (eds) Influence of climate change on the changing Arctic and sub-Arctic conditions. Springer, Heidelberg, p 73–93

van Franeker JA, Flores H, Van Dorssen M (2009) The surface and under ice trawl (SUIT). Frozen desert alive — the role of sea ice for pelagic macrofauna and its predators. PhD thesis, University of Groningen, Groningen

Wassmann P, Duarte CM, Agust ÍS, Sejr MK (2011) Footprints of climate change in the Arctic marine ecosystem. Glob Change Biol 17:1235–1249

Welch HE, Bergmann MA, Siferd TD, Martin KA and others (1992) Energy flow through the marine ecosystem of the Lancaster Sound Region, Arctic Canada. Arctic 45: 343–357

Werner I (1997) Grazing of Arctic under-ice amphipods on sea-ice algae. Mar Ecol Prog Ser 160:93–99

Werner I, Arbizu MP (1999) The sub-ice fauna of the Laptev Sea and the adjacent Arctic Ocean in summer 1995. Polar Biol 21:71–79

Werner I, Auel H (2005) Seasonal variability in abundance, respiration and lipid composition of Arctic under-ice amphipods. Mar Ecol Prog Ser 292:251–262

Werner I, Gradinger R (2002) Under-ice amphipods in the Greenland Sea and Fram Strait (Arctic): environmental controls and seasonal patterns below the pack ice. Mar Biol 140:317–326

Zuur AF, Ieno EN, Smith GM (2007) Analysing ecological data, Vol 680. Springer, New York, NY

Editorial responsibility: James McClintock, Birmingham, Alabama, USA

Submitted: July 2, 2014; Accepted: December 4, 2014
Proofs received from author(s): February 20, 2015